NANO LETTERS

2007
Vol. 7, No. 11
3528−3534

Wiring-Up Hydrogenase with Single-Walled Carbon Nanotubes

Timothy J. McDonald, Drazenka Svedruzic, Yong-Hyun Kim, Jeffrey L. Blackburn, S. B. Zhang, Paul W. King,* and Michael J. Heben*

Energy Sciences, National Renewable Energy Laboratory, Golden, Colorado 80401

Received September 10, 2007

ABSTRACT

Many envision a future where hydrogen is the centerpiece of a sustainable, carbon-free energy supply. For example, the energy in sunlight may be stored by splitting water into H_2 and O_2 using inorganic semiconductors and photoelectrochemical approaches[1] or with artificial photosynthetic systems that seek to mimic the light absorption, energy transfer, electron transfer, and redox catalysis that occurs in green plants.[2] Unfortunately, large scale deployment of artificial water-splitting technologies may be impeded by the need for the large amounts of precious metals required to catalyze the multielectron water-splitting reactions. Nature provides a variety of microbes that can activate the dihydrogen bond through the catalytic activity of [NiFe] and [FeFe] hydrogenases,[3,4] and photobiological approaches to water splitting have been advanced.[5] One may also consider a biohybrid approach; however, it is difficult to interface these sensitive[6,7] metalloenzymes to other materials and systems. Here we show that surfactant-suspended carbon single-walled nanotubes (SWNTs) spontaneously self-assemble with [FeFe] hydrogenases in solution to form catalytically active biohybrids. Photoluminescence excitation and Raman spectroscopy studies show that SWNTs act as molecular wires to make electrical contact to the biocatalytic region of hydrogenase. Hydrogenase mediates electron injection into nanotubes having appropriately positioned lowest occupied molecular orbital levels when the H_2 partial pressure is varied. The hydrogenase is strongly attached to the SWNTs, so mass transport effects are eliminated and the absolute potential of the electronic levels of the nanotubes can be unambiguously measured. Our findings reveal new nanotube physics and represent the first example of "wiring-up" an hydrogenase with another nanoscale material. This latter advance offers a nonprecious metal route to the design of new biohybrid architectures and building blocks for hydrogen-related technologies.

Introduction. Hydrogenases are comprised of a polypeptide chain and abundant first-row transition metals and are being explored for use in H_2 production and as catalysts in biofuel cells.[8,9] Incorporating hydrogenases into electrical devices is hampered by the difficulty of establishing a robust electrical connection between the enzyme and a support in a manner that does not compromise catalytic activity. Single-walled carbon nanotubes (SWNTs) are promising candidates for this job because they are nanoscale molecular wires with outstanding electrical conductivity and have shown the ability to form complexes with biological species. For example, SWNTs interacting with peroxidase[10] and glucose oxidase[11,12] have been employed in biosensing studies, and complexes of SWNTs with photosynthetic proteins are able to stabilize charge-transfer states.[13] Moreover, enzymes show improved stabilities to heat and solvent denaturation when in a complex with SWNTs.[14]

To study hydrogenase-SWNT interactions we selected the [FeFe] hydrogenase I (*Ca*HydI) from the anaerobic bacterium *Clostridium acetobutylicum*. *Ca*HydI has recently become readily available with the development of efficient preparation and purification processes.[15,16] Recombinant *Ca*HydI was overexpressed in *E. coli* and purified as previously described.[15] Neither *Ca*HydI nor the SWNTs were specially modified to facilitate formation of complexes. To prepare solutions in which SWNT and *Ca*HydI could interact, we simply mixed *Ca*HydI and SWNT/surfactant suspensions in 50−100 mM TES buffer (pH 7). All preparations were previously equilibrated under a 4% H_2 in N_2 atmosphere and sealed in airtight cuvettes to maintain anaerobic conditions. For more information about the SWNT materials and the methods used to assay hydrogenase catalytic activity, please see Supporting Information.

To evaluate the interaction between SWNTs and *Ca*HydI, we employed photoluminescence (PL) spectroscopy. PL from semiconducting SWNTs was first observed in 2002 when tubes were isolated in solution by aqueous surfactants.[17] Since that time PL excitation (PLE) spectroscopy has become a powerful tool for probing the optoelectronic properties of SWNT samples. For example, SWNT PL is extremely sensitive to pH[18,19] and changes in the dielectric environment[20,21] and is quenched by electron transfer to molecular acceptors.[11,22] Time-dependent changes in the PL signals can also be used to measure rebundling kinetics and to probe the strength of binding between surfactants and SWNTs as a function of tube diameter.[23]

* Corresponding authors. E-mail: (M.J.H) michael_heben@nrel.gov; (P.W.K) paul_king@nrel.gov. Phone: 303-384-6641. Fax: 303-384-6432.

10.1021/nl072319o CCC: $37.00
Published on Web 10/30/2007

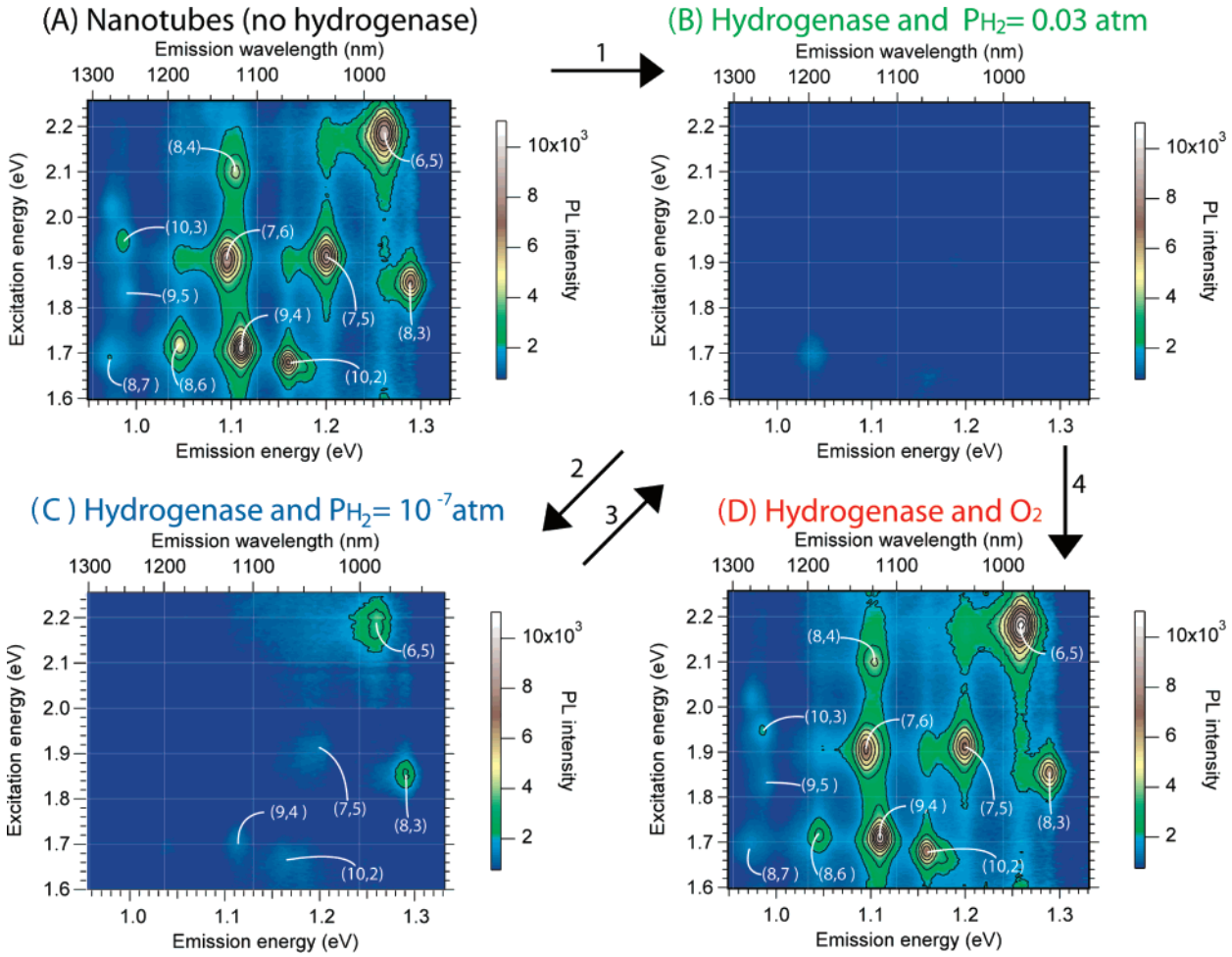

Figure 1. Contour maps of PL from nanotubes suspended in sodium cholate surfactant (A) without any added *Ca*HydI, (B) with added *Ca*HydI at a final concentration of ~1 μg/mL in the presence of H_2 (P_{H_2} = 0.03 atm) but no O_2, (C) after H_2 in panel B is replaced by Ar ($P_{H_2} = 10^{-7}$ atm), and (D) with the sample from panel B exposed to air. The arrows denote the order of experiments. The nanotube PL was excited at E_2 and detected at E_1, as described in the text.

Results. We measured PLE contour maps with a customized Thermo-Electron FT960 Raman spectrometer equipped with a Ge detector operating at 77 K.[24] The excitation source was a 250 W tungsten−halogen bulb coupled to a single-grating monochromator (the excitation intensity was <1 mW). All spectra were corrected for intensity variations in the lamp spectrum as well as for the responses of the system and detector. Figure 1A shows the contour map for the starting nanotube suspension. Each bright spot indicates emission from a specific nanotube of (n,m) index as assigned by Weisman et al.[25,26] The PL contour map for the SWNTs equilibrated with the H_2/N_2 atmosphere was indistinguishable from the data obtained prior to excluding air (Figure 1A). However, when active *Ca*HydI and SWNTs were combined, *Ca*HydI displaced surfactant (*vide infra*), adsorbed onto the SWNTs surfaces, and efficiently quenched the SWNT PL emission from all tubes (Figure 1B). The SWNT PL remained quenched for the duration of observation (at least one week) as long as anaerobic conditions were maintained. Notably, the presence of SWNTs did not adversely affect the assayed catalytic activity of *Ca*HydI when cholate concentrations in the mixture were kept below 0.4% (w/v) (see Supporting Information). Higher cholate concentrations denatured and irreversibly deactivated *Ca*HydI.

*Ca*HydI is comprised of two functional types of FeS-clusters: a catalytic H-cluster and electron-transfer F-cluster.[4] We note that SWNT optical properties were not affected when nanotube suspensions were mixed with *Ca*HydI that contained only the electron transfer F-cluster or when nanotubes were mixed with just the storage buffer or solutions containing oxidized or denatured *Ca*HydI. Thus, the changes in nanotube PL were observed only when complexes were formed with catalytically active *Ca*HydI.

PL from SWNTs can be lost due to tube aggregation,[17,23] contact with substrates,[27] changes in pH,[18] covalent functionalization,[28] or redox processes.[11,22] Because we investigated solutions that were quite stable and homogeneous and the pH was buffered, we can immediately disregard the first three possibilities. Covalent functionalization can also be discounted because nanotubes are inherently unreactive under the mild, room-temperature conditions employed here. However, to probe this possibility in more detail we investigated optical absorption spectra before and after SWNT−*Ca*HydI complex formation (Figure 2). As is well

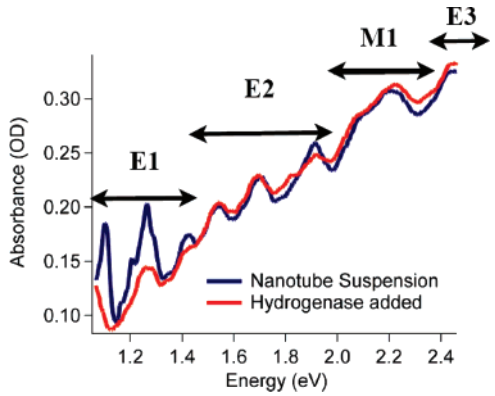

Figure 2. Absorption spectra of single-walled carbon nanotubes suspended in sodium cholate surfactant with and without the *Ca*HydI hydrogenase under a H_2 partial pressure of 0.03 atm. Linear absorption (OD) measurements were taken using a Cary 500 spectrometer with a 1 cm path length cell. The effect of *Ca*HydI addition is consistent with reduction of all semiconducting nanotubes present, as the lowest energy nanotube transitions (E_1) at ~1.0−1.3 eV have been reduced in concert with the loss of PL emission.

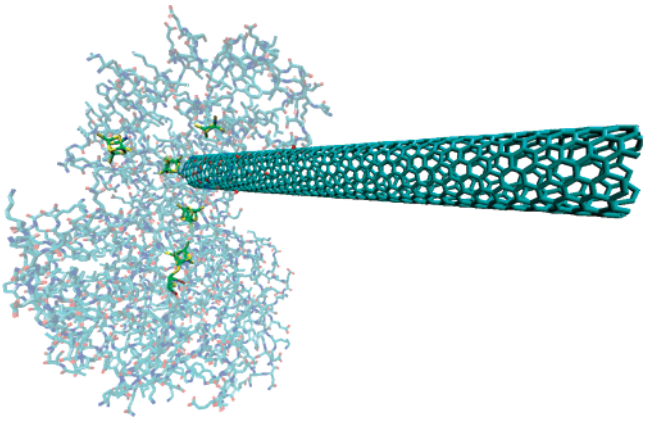

Figure 3. Molecular model of *Ca*HydI bound to a SWNT.[31] The yellow and green units show the FeS clusters. This conformation was selected as one plausible arrangement for the complex among several based on geometric fit, because in this example the SWNT surface lies close to one of the electron-transfer F-clusters of *Ca*HydI. There are many possible geometries, but the existence of a strong electronic interaction demonstrates that at least one of the FeS clusters must be proximal to the tubes.

known, the cylindrical sp^2-bonded carbon network of SWNTs gives rise to distinct absorption features associated with the allowed transitions between the van Hove singularities.[29] Covalent functionalization would lead to the appearance of new absorption features and the disappearance of both the first (E_1) and second (E_2) excitonic transitions in the affected nanotubes. Instead, only a bleaching of the E_1 transitions are seen, and the E_2 transitions are not significantly perturbed. This change in the oscillator strength at E_1 is expected for either electron or hole injection at the band edges. Because the E_1 absorption features are not shifted upon interaction with hydrogenase, one can rule out the formation of a hybrid electronic structure deviating significantly from that of the components. Thus, redox processes are the likely cause of the PL quenching observed in our experiments.

O'Connell et al. observed PL quenching when SDS-stabilized SWNTs were exposed to molecular acceptors in solution and attributed the quenching to holes left in the tube's valence band (i.e., the highest occupied molecular orbital (HOMO)) after electron transfer.[22] These holes quench SWNT PL through Auger recombination processes[19] as is seen when excess charge carriers (either electrons or holes) are present in colloidal semiconductor nanocrystals.[30] Our results are similar accept for two important differences: (i) under the reducing conditions employed here, the SWNT PL is evidently quenched by electron injection, and (ii) *Ca*HydI is a biocatalyst that can establish equilibrium between the SWNTs and the potential of the $2H^+ + 2e^- \rightarrow H_2$ (H^+/H_2) half-reaction. The simple observation that the *Ca*HydI must be catalytically active to observe PL quenching and that the quenching is reversible with changes in the redox potential of the H^+/H_2 half-reaction (*vide infra*) demonstrates that the enzyme mediates and establishes the equilibrium. Thus, it seems clear that the enzyme must be adsorbed with either the H-cluster or one of the electron relay FeS-clusters in intimate contact with the SWNT surface. The assertion that charge transfer is responsible for the PL quenching is further proven by Raman spectroscopy data (see Supporting Information). The fact that the PL quenching occurs only under reducing conditions establishes that electron injection into the tube's lowest unoccupied molecular orbital (LUMO) is responsible, rather than electron transfer from the tube's HOMO to acceptor redox species.[22]

Figure 3 shows a molecular model of a possible arrangement for the biohybrid complex.[31] As discussed previously, *Ca*HydI is able to shuttle electrons into the LUMOs of all of the monitored semiconducting SWNTs, resulting in complete quenching of the PL (Figure 1B) and partial bleaching of the E_1 optical absorption (Figure 2) when the hydrogen partial pressure, P_{H_2}, is 0.03 atm (i.e., 4% H_2 at 620 Torr, which is atmospheric pressure in Golden, CO). The fact that efficient PL quenching is observed while the absorption transitions are only partially bleached is in complete agreement with a previous report for SWNTs, which showed that the number of charges necessary to completely bleach the absorption spectra is more than an order of magnitude larger than that required to fully quench PL.[19] This may be understood by considering that the intensity of the absorption spectra and related bleaching scales with the number of carbon atoms and injected carriers, respectively, while a single excess charge can cause the nonradiative recombination of many excitons. Complete bleaching of the E_1 transitions would be expected only if multiple electron-transfer events fully populated the SWNT LUMOs. However, this is not observed, presumably due to band shifting and coulomb blockade effects.

The electrochemical potential of the H^+/H_2 redox couple and the catalytic apparatus of *Ca*HydI may be tuned by adjusting either the pH or the H_2 partial pressure. To investigate if the formation of *Ca*HydI−SWNT complexes render the SWNT PL responsive to the redox potential of the H^+/H_2 couple, we removed H_2 from the pH 7 solution by three evacuation/backfill cycles using Ar to replace the H_2/N_2 atmosphere. After 24 h under the low P_{H_2} conditions

($\sim 10^{-7}$ atm), another PL map of the suspension was collected (Figure 1C). Interestingly, the PL was restored for the (8,3) and (6,5) species that have the highest emission energies and the smallest diameters, while the lowest energy-emitting, largest diameter tubes remained dark. Weak PL was observed for the (7,5), (10,2), and (9,4) tubes that emit on the high-energy side of the distribution. Qualitatively, the findings are explained by considering that the H^+/H_2 redox couple moves to more positive potentials with the lowering of P_{H_2} and, as a result electrons are no longer able to be injected into the LUMOs of all tubes by *Ca*HydI-catalyzed H_2 oxidation. Electrons may transfer back from tubes having LUMOs that are more reducing than the new potential of the H^+/H_2 couple, and these tubes can emit PL once again. Note that the PL bleaching is completely reversible; the PL contour plot reverts from Figure 1C to Figure 1B when P_{H_2} is restored to 0.03 atm. In contrast, when the solution is exposed to atmospheric O_2 ($P_{O_2} = 0.17$ atm), which irreversibly deactivates the H-cluster, all nanotubes are once again observed in the PL contour map (Figure 1D).

Discussion. To understand the results in more detail, we consider where the energies of the SWNTs LUMO levels lie relative to vacuum as a function of the (n,m) index. The absolute potentials of the Fermi levels for several SWNTs were calculated by Shan and Cho and found to be relatively constant with diameter and band gap.[32] If this result is correct, then the HOMO and LUMO levels should open up in energy relatively symmetrically about a constant value with increasing band gap (decreasing diameter). In contrast, earlier experimental studies concluded that the Fermi level position of SWNTs varied strongly as a function of band gap, suggesting that both the HOMO and LUMO levels moved to lower energy with increasing band gap.[22,33] However, these studies were likely affected by tube-dependent surfactant lability and related mass-transport effects, which have only recently become known.[23] In the present case, the *Ca*HydI is strongly bound to the SWNTs, so mass transport effects are not expected to be significant.

Because the SWNTs investigated by Shan and Cho[32] were not the same as the ones present in our preparations, we performed our own density functional theory (DFT) calculations within the local density approximation (LDA) to locate the individual Fermi levels (see Supporting Information). The electronic bandgaps were determined by adding the optical band gaps measured in Figure 1 to the exciton binding energies reported by Dukovic et al.[34] One-half of the electronic band gap value was then added to the calculated LDA Fermi energy to determine the LDA LUMO positions (Table 1). In agreement with Shan and Cho,[32] the Fermi levels for the SWNTs investigated here vary by only ±40 meV. If we used the LDA LUMO positions to explain why the (6,5) PL restores and why the (8,4) PL remains dark at low-hydrogen pressure, the H^+/H_2 redox level should be located between the LUMOs of the (6,5) and (8,4) tubes, that is, at approximately -3.74 ± 0.05 eV. However, the Nernst equation indicates the redox potential to be −4.24 eV. The difference of 0.5 eV may be due to the vacuum approximation that we used for solution environment. In any event, it is clear that the LDA values need to be corrected by −0.5 eV. The corrected Fermi levels are close to those in the literature.[35,36]

Table 1. Fermi Level and LUMO vs Vacuum of Semiconducting Single-Walled Nanotubes as Determined by the DFT−LDA Method

(n,m)	diameter (nm)	Fermi level LDA (eV)	electronic band gap (eV)[a]	LUMO LDA (eV)	LUMO expt (eV)[b]
(6,5)	0.76	−4.536	1.69	−3.691	−4.19
(8,3)	0.78	−4.469	1.71	−3.614	−4.11
(8,4)	0.84	−4.549	1.51	−3.794	−4.29
(10,2)	0.88	−4.481	1.5	−3.731	−4.23
(7,6)	0.9	−4.515	1.45	−3.790	−4.29
(8,6)	0.97	−4.514	1.4	−3.814	−4.31
(10,5)	1.05	−4.501	1.3	−3.851	−4.35
graphite		−4.486			

[a] Determined by adding optical band gap to the exciton binding energies reported by Dukovic et al.[34] [b] In accordance with the redox potentials determined by the Nernst equation, the LDA LUMO values are corrected by −0.5 eV. The error is ±0.05 eV.

Figure 4 shows the corrected LUMO and HOMO levels for selected SWNTs plotted as a function of decreasing tube diameter. The levels are plotted on an absolute energy scale as well as on the electrochemical scale where zero is −4.44 eV versus vacuum.[37] Also shown are horizontal lines corresponding to the electrochemical potential of the H^+/H_2 redox couple under the high ($P_{H_2} = 0.03$ atm) and low ($P_{H_2} \sim 10^{-7}$ atm) H_2 partial pressures. The corresponding electrochemical potentials (−4.07 and −4.24 eV, respectively) were determined from the Nernst equation with the known values of pH, P_{H_2}, and temperature. Figure 4 explains how changing the potential of the H^+/H_2 redox couple affects the SWNT PL. When P_{H_2} is 0.03 atm, the potential of the H^+/H_2 redox couple is more negative (on the electrochemical scale) than the LUMO levels of all tubes. Adsorbed *Ca*HydI is thus able to shuttle electrons into the LUMO of each tube, effectively reducing the tubes by catalyzing H_2 oxidation. This bleaches the PL emission (Figure 1B). When P_{H_2} is reduced to 10^{-7} atm, the H^+/H_2 redox couple moves more positive and electrons are no longer injected into the smaller diameter tubes. The smallest nanotubes, the (8,3) and (6,5) species, have LUMO levels that are significantly more negative than the equilibrated *Ca*HydI potential, and thus their PL is strongly restored. The (9,4), (7,5), and (10,2) species are somewhat larger and their LUMOs are very near the potential of the H^+/H_2 couple at $P_{H_2} \sim 10-7$ atm. Thus, their PL is only weakly restored (Figure 1C). The largest diameter tubes remain reduced and do not emit PL until the solution is exposed to ambient levels of O_2 in lab air. Exposure to O_2 irreversibly oxidizes the H-cluster and disrupts the ability of *Ca*HydI to equilibrate the SWNTs with the potential of the H^+/H_2 redox couple. This results in complete restoration of the PL of all tubes (Figure 1D). We schematically represent this condition in Figure 4 with the horizontal labeled $P_{O_2} = 0.17$ atm. The reducing equivalents on the SWNTs are evidently removed either by competing against the oxidation of the FeS clusters by air or possibly via reactions with the O_2/H_2O redox couple as has been reported by Zheng and Diner.[38]

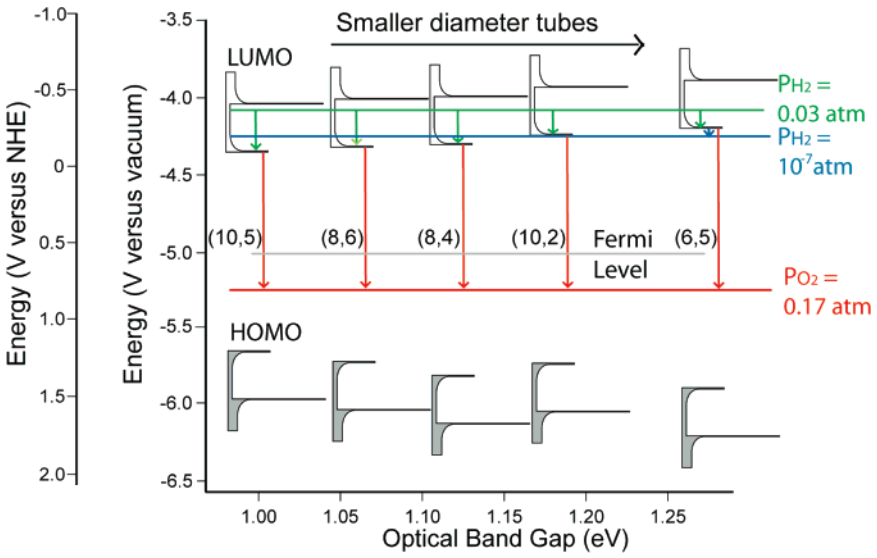

Figure 4. Diagram of nanotube LUMO and HOMO levels vs optical band gap and decreasing nanotube diameter determined as described in the text. The electrochemical potential of the H^+/H_2 redox couple is shown for two P_{H_2} values, along with the potential of the O_2/H_2O redox couple for a P_{O_2} value.

Additional information regarding the strength and nature of the *Ca*HydI−SWNT interaction can be obtained from consideration of the rates at which the tube-specific PL changes.[23] Figure 5A shows the rate of PL loss for the (7,6) tube after the SWNT and active *Ca*HydI solutions are first mixed under 0.03 atm H_2 at room temperature (circles) compared to when the concentration of the sodium cholate surfactant concentration for a pure SWNT solution is diluted 25-fold at 50 °C (squares). In the latter case, the PL is lost due to rebundling of tubes.[23] An elevated temperature was required to observe the quench on a time scale comparable to the *Ca*HydI-induced PL quench. As we showed previously, the cholate surfactant is rather strongly bound to the SWNTs surfaces.[23] The fact that the PL quench due to *Ca*HydI occurs much more rapidly, even at room temperature, demonstrates that *Ca*HydI binds more strongly and displaces the sodium cholate to gain access to the SWNT surface.

The PL decay for the (7,6) tube and all other observed tubes (see Supporting Information) after addition of active *Ca*HydI is well fit by the integrated form of a first-order rate equation, where I_{io} is the initial intensity of the i_{th} species (eq 1)

$$\frac{I_i}{I_{io}} = \exp\{-k_i \cdot t\} \tag{1}$$

Figure 5B shows the k_i rate constants for each nanotube in the distribution plotted as a function of emission energy, which scales inversely with diameter. The decay rate is diameter-dependent with the PL decaying from the largest (lowest emission energy) nanotubes most quickly. We previously showed that the binding energy of cholate surfactant to SWNTs is also diameter-dependent with the largest diameter tubes binding the surfactant most weakly.[23] The diameter-dependence of the quench is consistent with the cholate surfactant being more readily displaced from the larger diameter tubes, but the difference in the rate of interaction as seen in Figure 5A suggests that another factor may be at play. Rate theory predicts that the rate constant for charge transfer should depend exponentially on the electrochemical driving force (ΔG). The magnitude of ΔG in our experiments is the potential difference between the H^+/H_2 redox potential and the LUMO of each nanotube. To determine if the observed quenching kinetics are governed by the electrochemical driving force, we plotted $\ln(k_i)$ versus ΔG for each tube and fit the data according to eq 2

$$\ln(k_i) = -\frac{M\Delta G}{KT} + C \tag{2}$$

where K is the Boltzmann constant, T is the temperature, and M is a factor that can be adjusted to obtain the best fit. If, for example, the decay rate is governed solely by the electrochemical driving force, and there is no other diameter-dependent factor in the decay rate, then the value of M should be unity. For the initial decay of the nanotube PL upon the addition of active *Ca*HydI, we find a value of 0.18 for M. Thus, the decay rate is less sensitive to diameter than if it were determined solely by the electrochemical driving force, which could be explained by the need for *Ca*HydI to displace surfactant to gain access to the SWNT surface when the two components are first mixed.

When P_{H_2} is reduced to 10^{-7} atm, we can measure the time dependence of the reappearance of PL from the five tube species seen in Figure 1C. In this case the return of the PL is well fit by the equation

$$\frac{I_i}{I_{io}} = 1 - \exp\{-r_i \cdot t\} \tag{3}$$

Figure 5B (squares) plots the fit PL return constants, r_i, which

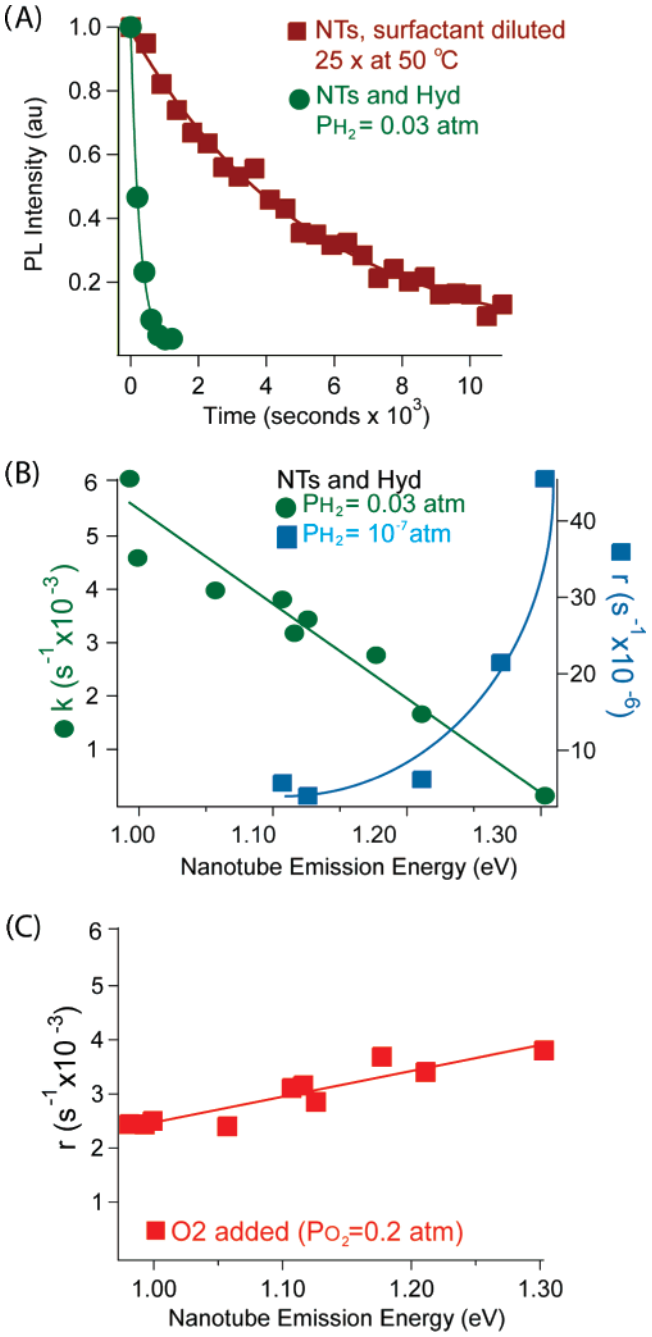

Figure 5. (A) PL emission intensity for the (7,6) nanotube as a function of time after *Ca*HydI is added to the SWNT suspension (circles) and a pure SWNT suspension (no *Ca*HydI) is diluted 25-fold and heated to 50 °C (squares). (B) Individual nanotubes' rate of PL bleaching upon *Ca*HydI addition (k, circles) and the rate of PL return when the H_2 partial pressure is reduced (r, squares) versus nanotube emission energy. (C) Individual nanotubes' rate of PL recovery (r) upon exposure to atmospheric O_2 versus nanotube emission energy. The rates are obtained by fitting the progress curve data for each nanotube to first-order exponential functions. The lines in (A) are fit exponential functions and the lines in (B) and (C) are guides to the eye. (For more detailed explanation see "kinetic model" in Supporting Information).

were determined for the five nanotubes whose PL returned upon removal of H_2. In contrast to the PL bleaching, the rate of return is strongly dependent on the emission energy and is fastest for the (8,3) nanotube, which is the smallest tube in the distribution. Analyzing the return rate (r) in Figure 5B in an analogous manner as was done for the bleach rate constants, we find that the M factor is 1.106, a value that implies the diameter-dependence is determined solely by the electrochemical driving force, ΔG. This is a result of *Ca*HydI being already bound to the nanotube surface. In this case, mass transport of *Ca*HydI to and from the SWNT surface does not play a role, and the only change in the system is the H^+/H_2 redox potential. Because observation of the electrochemical properties of single-nanotube types can be accomplished without competing diameter-dependent surfactant binding and displacement effects, this approach is appropriate for determining the absolute potential of the nanotube LUMO levels, as was done in Figure 4.

As mentioned previously, exposure to atmospheric levels of O_2 ($P_{O_2} \sim 0.17$ atm) causes the PL for all nanotubes to return. The rate of PL intensity versus time for all tubes is again fit well by eq 3, and the rate of PL return versus nanotube band gap is shown in Figure 5C. The higher band gap nanotubes tend to have a higher r_i; in other words their PL returns more quickly than does the PL from the lower energy (larger diameter) nanotubes. The rate of H_2 production catalyzed by *Ca*HydI in the presence of SWNTs with the same conditions as those used for the PL experiment were measured in the presence of atmospheric O_2 by standard techniques (see Supporting Information). The rate of *Ca*HydI deactivation in aerobic conditions obtained by fitting the experimental data to eq 3 was 0.003 ± 0.001 s^{-1}, which is the same order of magnitude as the rates of the PL return (Figure 5C). The rate of PL return is not determined solely by the diffusion of O_2 into the vial and subsequent deactivation of catalytic center, in which case r_i would then be the same for all nanotubes. In fact, this result may be evidence for stronger *Ca*HydI binding to larger diameter tubes. If there are no other nanotube type-dependent effects, the rate of nanotube oxidation should be greatest for the nanotubes with the most energetic LUMOs. However, fitting $\ln(r_i)$ to eq 3 reveals an M value of only 0.091, which implies that diameter-dependence of the return of PL is reduced compared to the pure electrochemical driving force.

In conclusion, we have shown that surfactant isolated SWNTs can be used as molecular wires to make electrical contact to and from stable and functional complexes with [FeFe] hydrogenase I from *Clostridium acetobutylicum*. The complexes self-assemble and form spontaneously when surfactant is displaced and *Ca*HydI is adsorbed onto SWNT surface. The hydrogenase remains catalytically active so long as anaerobic conditions are maintained. The absolute potential of the Fermi level for a range of semiconducting SWNTs was found to be -5.0 eV relative to the vacuum level and varied little with diameter. Thus, the SWNTs LUMO levels are more positive in energy with increasing nanotube band gap. By carefully designed synthesis, it should be possible to tune the catalytic biohybrids for use as electrochemical probes for in vivo detection of hydrogenase activities. More importantly, this work offers the first step toward the construction of functional hydrogenase/SWNT hybrids for

application in a variety of hydrogen production and fuel cell technologies.

Acknowledgment. The authors are grateful for support from the U.S. Department of Energy, Office of Science, Office of Basic Energy Sciences, Division of Chemical Sciences, Geosciences, and Biosciences.

Supporting Information Available: Materials and methods, kinetic mechanisms, Raman spectra, and PL emission intensity. This material is available free of charge via the Internet at http://pubs.acs.org.

References

(1) Khaselev, O.; Turner, J. A. *Science* **1998**, *280* (5362), 425−427.
(2) Alstrum-Acevedo, J. H.; Brennaman, M. K.; Meyer, T. J. *Inorg. Chem.* **2005**, *44* (20), 6802−6827.
(3) Volbeda, A.; Charon, M.-H.; Piras, C.; Hatchikian, E. C.; Frey, M.; Fontecilla-Camps, J. C. *Nature* **1995**, *373* (6515), 580−587.
(4) Peters, J. W.; Lanzilotta, W. N.; Lemon, B. J.; Seefeldt, L. C. *Science* **1998**, *282* (5395), 1853−1858.
(5) Ghirardi, M. L.; Posewitz, M. C.; Maness, P.-C.; Dubini, A.; Yu, J.; Seibert, M. *Annu. Rev. Plant Biol.* 2007, 58 (1).
(6) Adams, M. W. W. *Biochim. Biophys. Acta* **1990**, *1020* (2), 115−145.
(7) Adams, M. W. W.; Mortenson, L. E.; Chen, J.-S. *Biochim. Biophys. Acta* **1980**, *594* (2−3), 105−176.
(8) Vincent, K. A.; Cracknell, J. A.; Lenz, O.; Zebger, I.; Friedrich, B.; Armstrong, F. A. *Proc. Natl. Acad. Sci. U.S.A.* **2005**, *102* (47), 16951−16954.
(9) Wenk, S. O.; Qian, D. J.; Wakayama, T.; Nakamura, C.; Zorin, N.; Rogner, M.; Miyake, J. *Int. J. Hydrogen Energy* **2002**, *27* (11−12), 1489−1493.
(10) Yu, X.; Chattopadhyay, D.; Galeska, I.; Papadimitrakopoulos, F.; Rusling, J. F. *Electrochem. Commun.* **2003**, *5* (5), 408−411.
(11) Barone, P. W.; Baik, S.; Heller, D. A.; Strano, M. S. *Nat. Mater.* **2005**, *4*, 86−92.
(12) Song, C. H.; Pehrsson, P. E.; Zhao, W. *J. Mater. Res.* **2006**, *21* (11), 2817−2823.
(13) Dorogi, M.; Balint, Z.; Miko, C.; Vileno, B.; Milas, M.; Hernadi, K.; Forro, L.; Varo, G.; Nagy, L. *J. Phys. Chem. B* **2006**, *110* (43), 21473−21479.
(14) Asuri, P.; Karajanagi, S. S.; Yang, H.; Yim, T. J.; Kane, R. S.; Dordick, J. S. *Langmuir* **2006**, *22*, 5833−5836.
(15) King, P. W.; Posewitz, M. C.; Ghirardi, M. L.; Seibert, M. *J. Bacteriol.* **2006**, *188* (6), 2163−2172.
(16) Posewitz, M. C.; King, P. W.; Smolinski, S. L.; Zhang, L.; Seibert, M.; Ghirardi, M. L. *J. Biol. Chem.* **2004**, *279* (24), 25711−25720.
(17) O'Connell, M. J.; Bachilo, S. M.; Huffman, C. B.; Moore, V. C.; Strano, M. S.; Haroz, E. H.; Rialon, K. L.; Boul, P. J.; Noon, W. H.; Kittrell, C.; Ma, J. P.; Hauge, R. H.; Weisman, R. B.; Smalley, R. E. *Science* **2002**, *297* (5581), 593−596.
(18) Strano, M. S.; Huffman, C. B.; Moore, V. C.; O'Connell, M. J.; Haroz, E. H.; Hubbard, J.; Miller, M.; Rialon, K.; Kittrell, C.; Ramesh, S.; Hauge, R. H.; Smalley, R. E. *J. Phys. Chem. B* **2003**, *107* (29), 6979−6985.
(19) Dukovic, G.; White, B. E.; Zhou, Z. Y.; Wang, F.; Jockusch, S.; Steigerwald, M. L.; Heinz, T. F.; Friesner, R. A.; Turro, N. J.; Brus, L. E. *J. Am. Chem. Soc.* **2004**, *126* (46), 15269−15276.
(20) Strano, M. S.; Moore, V. C.; Miller, M. K.; Allen, M. J.; Haroz, E. H.; Kittrell, C.; Hauge, R. H.; Smalley, R. E. *J. Nanosci. Nanotechnol.* **2003**, *3* (1−2), 81−86.
(21) Heller, D. A.; Jeng, E. S.; Yeung, T. K.; Martinez, B. M.; Moll, A. E.; Gastala, J. B.; Strano, M. S. *Science* **2006**, *311* (5760), 508−511.
(22) O'Connell, M. J.; Eibergen, E. E.; Doorn, S. K. *Nat. Mater.* **2005**, *4* (5), 412−418.
(23) McDonald, T. J.; Engtrakul, C.; Jones, M.; Rumbles, G.; Heben, M. J. *J. Phys. Chem. B* **2006**, *110*, 25339.
(24) McDonald, T. J.; Jones, M.; Engtrakul, C.; Ellingson, R. J.; Rumbles, G.; Heben, M. J. *Rev. Sci. Instrum.* **2006**, *77*, 053104.
(25) Weisman, R. B.; Bachilo, S. M. *Nano Lett.* **2003**, *3* (9), 1235−1238.
(26) Weisman, R. B.; Bachilo, S. M.; Strano, M. S.; Kittrell, C.; Hauge, R. H.; Smalley, R. E. *AIP Conf. Proc.* **2003**, *685*, 241−245.
(27) Lefebvre, J.; Austing, D. G.; Bond, J.; Finnie, P. *Nano Lett.* **2006**, *6* (8), 1603−1608.
(28) Bahr, J. L.; Tour, J. M. *J. Mater. Chem.* **2002**, *12* (7), 1952−1958.
(29) Dresselhaus, M. S.; Dresselhaus, G.; Saito, R. *Solid State Commun.* **1992**, *84*, 201.
(30) Shim, M.; Wang, C. J.; Guyot-Sionnest, P. *J. Phys. Chem. B* **2001**, *105* (12), 2369−2373.
(31) Note: To generate the possible geometric combinations of the nanotube and *Ca*HydI, we utilized *PatchDock*, a molecular docking algorithm based on shape complementary principles. http://bioinfo3d.cs.tau.ac.il/PatchDock/patchdock.
(32) Shan, B.; Cho, K. *Phys. Rev. Lett.* **2005**, *94* (23), 236602−4.
(33) Okazaki, K.; Nakato, Y.; Murakoshi, K. *Phys. Rev. B* **2003**, *68* (3).
(34) Dukovic, G.; Wang, F.; Song, D.; Sfeir, M. Y.; Heinz, T. F.; Brus, L. E. *Nano Lett.* **2005**, *5* (11), 2314−2318.
(35) Shiraishi, M.; Ata, M. *Carbon* **2001**, *39* (12), 1913−1917.
(36) Suzuki, S.; Bower, C.; Watanabe, Y.; Zhou, O. *Appl. Phys. Lett.* **2000**, *76* (26), 4007−4009.
(37) Bockris, J. O. M.; Reddy, A. K. N.; Gamboa-Aldeco, M., *Modern Electrochemistry*, 2nd ed.; Kluwer Academic/Plenum Publishers: New York, 2000; Volume 2A.
(38) Zheng, M.; Diner, B. A. *J. Am. Chem. Soc.* **2004**, *126* (47), 15490−15494.

NL072319O